Local gyrokinetic turbulence simulations with realistic tokamak geometries towards ITER and JT-60SA

[1]M. Nakata, [1]A. Matsuyama, [1]N. Aiba, [1]S. Maeyama

in collaboration with [2]T. -H. Watanabe, [2]H. Sugama, and [2]M. Nunami

[1]Japan Atomic Energy Agency

[2]National Institute for Fusion Science

NEXT workshop at Kyoto univ. August 29-30th, 2013

Outline

- Introduction
- Current status of local gyrokinetic Vlasov code GKV
- Interface between MEUDAS(2D equilibrium solver) and GKV
- Application to realistic plasma shapes on JT-60SA
  - Linear ITG mode stability
  - Residual zonal flow levels
  - Nonlinear zonal flow generations
- Summary

Introduction

- Turbulent transport properties can be strongly affected by the plasma shaping effects, through the change of the linear frequencies, mode-structures, and trapped/passing boundary.

Impact of the negative triangularity on stabilization of TEMs: global-GK analyses for TCV shape.
Camenen et al., NF2007

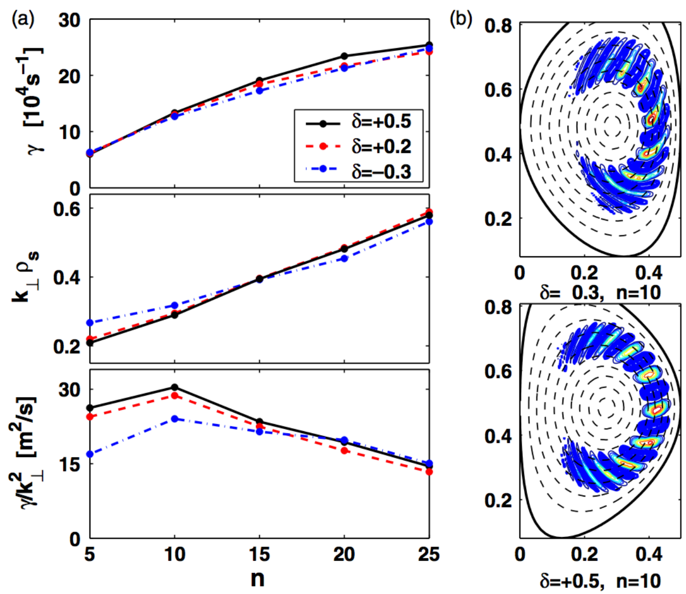

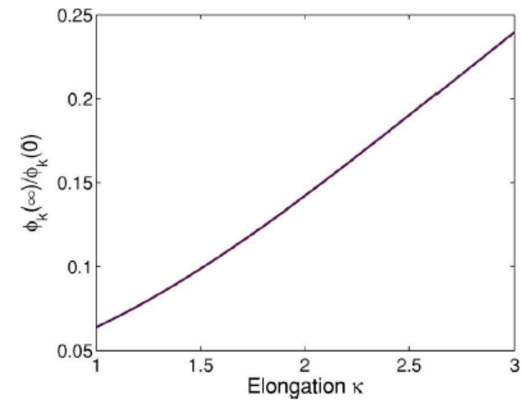

Enhanced residual-ZF levels by plasma elongation: Analytic analyses for Solove'v like equilibrium. Xiao and Catto, PoP2006

- Implementation of realistic shaped MHD-equilibrium to gyrokinetic code is useful for analyzing plasma shape effects, and for validation/prediction study against experiments.

---> In this study, tokamak equilibria calculated by a free-boundary 2D Grad-Shafranov solver MEUDAS are incorporated into a local fluxtube gyrokinetic code GKV.

---> Micro-stability and zonal flow generation in several equilibria on JT-60SA are investigated.

Current status of GKV code

- Local fluxtube 5D gyrokinetic solver, originally developed by [T. -H. Watanabe, NF2006]

 ---> Solving the evolution of delta-f in 5D phase space

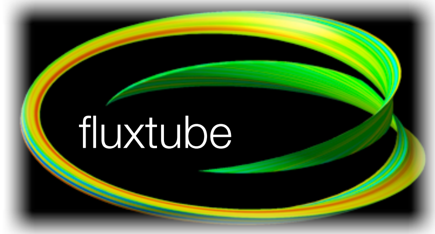

 ---> Eulerian (or Vlasov) solver: spectral in 2D k-space, Finite-Difference in 3D (z, $v_{||}$, μ)-space

 ---> Electro-static, Electro-magnetic, Arbitrary numbers of species

 ---> Helical geometries from VMEC, Tokamak geometries from MEUDAS(this talk)

 ---> Entropy balance/transfer diagnostics

[T. -H. Watanabe PRL2008, M. Nunami PFR2011, M. Nakata PoP2012, S. Maeyama CPC2013]

- GKV code is now ready for turbulence simulations of burning plasmas composed of D, T, e, He-ash, C, W, etc.

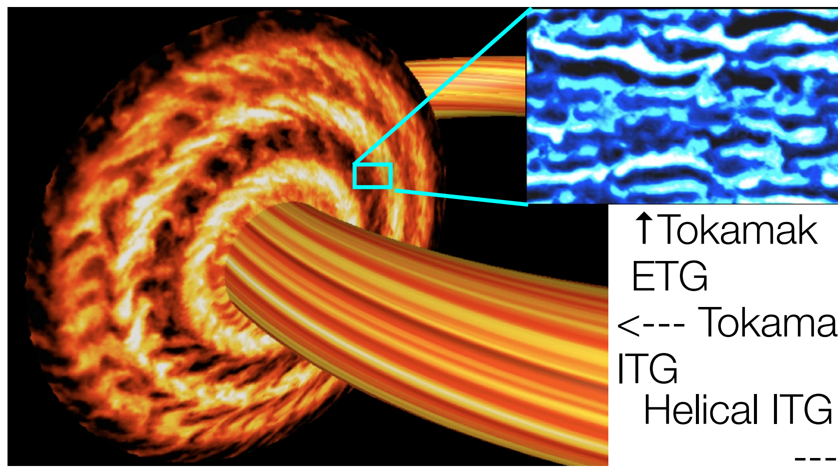

↑Tokamak ETG

<--- Tokamak ITG

Helical ITG --->

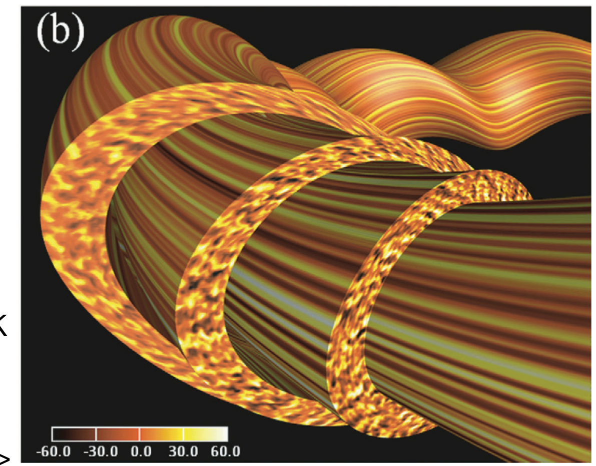

Advanced parallelization towards PETA/EXA computing

- 5D domain-decompositions with MPI and Thread parallelization with OPENMP

Decomposition in (z, $v_{\|}$, μ) + **Decomposition in k-space (kx or ky)** + **Species**

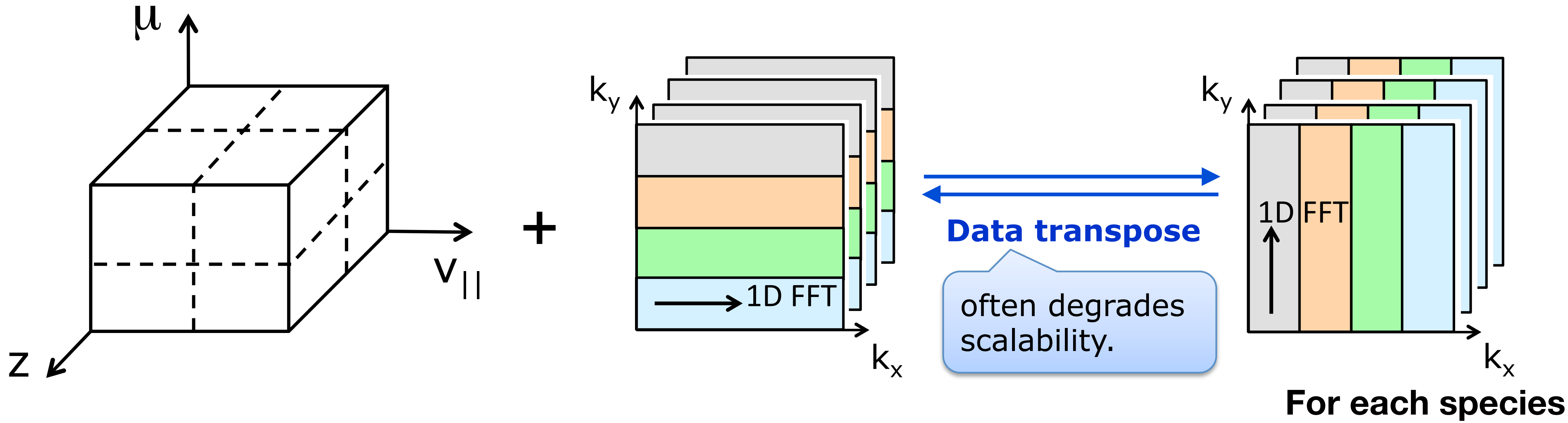

- Parallel 2D FFT (including data-transpose) for the nonlinear ExB advection term is the most time-consuming.

---> Segmented 3D rank-allocation technique (for MESH/TORUS network)

---> Communication/Computation Overlap technique (for FFT and/or FD)

[S. Maeyama, JSST2012 Y. Idomura, SC2012]

Fantastic scaling over 0.6M cores on K computer

Problem size for Multi-scale turbulence simulations (e.g. ITG-ETG)

N_x=1024, N_y=1024, N_z=128, N_v=64, N_μ=32 ~ 274 billion grids
P_k=8-64, P_z=16, P_v=8, P_μ=4, 8 threads > 600 thousand cores

Effects of Rank-Mapping and Overlap

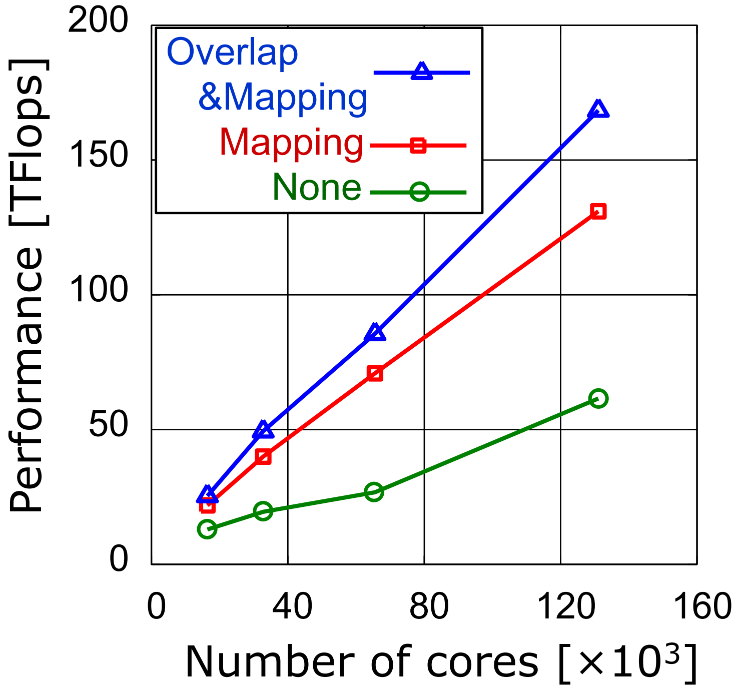

Strong scaling on K computer

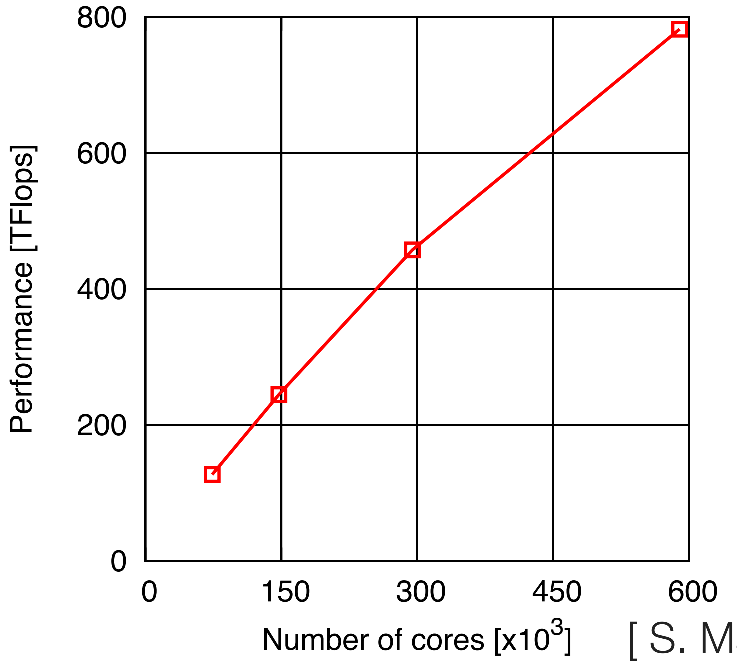

[S. Maeyama, SC2013]

Fantastic scalability over 0.6Mcores has been achieved with 99.99994% efficiency.

---> Multi-scale/Multi-species turbulence simulation is now accessible with GKV.

Outline

- Introduction
- Current status of local gyrokinetic Vlasov code GKV
- Interface between MEUDAS(2D equilibrium solver) and GKV
- Application to realistic plasma shapes on JT-60SA
  - Linear ITG mode stability
  - Residual zonal flow levels
  - Nonlinear zonal flow generations
- Summary

Gyrokinetic equation in flux coordinates

- Gyrokinetic and Poisson equations: electro-static limit, multi-species

$$\begin{cases} \left[\dfrac{\partial}{\partial t} + v_\parallel \boldsymbol{b}\cdot\nabla + i\boldsymbol{k}_\perp\cdot\boldsymbol{v}_{ds} - \dfrac{\mu}{m_s}\boldsymbol{b}\cdot\nabla B\dfrac{\partial}{\partial v_\parallel}\right]\delta f_{s\boldsymbol{k}_\perp} + \mathcal{N}(\delta f_{s\boldsymbol{k}_\perp}, \delta\psi_{s\boldsymbol{k}_\perp}) \\ \qquad = F_{Ms}\left[i\boldsymbol{k}_\perp\cdot\boldsymbol{v}_{*Ts} - i\boldsymbol{k}_\perp\cdot\boldsymbol{v}_{ds} - v_\parallel\boldsymbol{b}\cdot\nabla\right]\dfrac{e_s\delta\psi_{s\boldsymbol{k}_\perp}}{T_s} + C_s(h_{s\boldsymbol{k}_\perp}) \\ k_\perp^2\delta\phi_{\boldsymbol{k}_\perp} = 4\pi\sum_s e_s\left[\int d\boldsymbol{v}J_{0s}\delta f_{s\boldsymbol{k}_\perp} - n_{s0}\dfrac{e_s\delta\phi_{\boldsymbol{k}_\perp}}{T_s}(1-\Gamma_{0s})\right] \end{cases}$$

- Fluxtube coordinates (x, y, z) defined by general SFL flux coordinates (ρ, θ, ζ):

coordinates: $x = c_x(\rho - \rho_0),\ y = c_y[q(\rho)\theta - \zeta],\ z = \theta$

$\Psi = \Psi(\rho)$: poloidal flux

$\Phi = \Phi(\rho)$: toroidal flux

magnetic field: $\boldsymbol{B} = c_b\nabla x\times\nabla y,\ c_b = \dot{\Psi}/c_x c_y$

Jacobian: $\sqrt{g}_{xyz} = (\nabla x\times\nabla y\cdot\nabla z)^{-1} = (c_x c_y)^{-1}\sqrt{g}_{\rho\theta\zeta}$

Derivatives: $\dfrac{\partial}{\partial x} = \dfrac{1}{c_x}\dfrac{\partial}{\partial\rho} + \dfrac{\dot{q}(\rho)\theta}{c_x}\dfrac{\partial}{\partial\zeta},\quad \dfrac{\partial}{\partial y} = -\dfrac{1}{c_y}\dfrac{\partial}{\partial\zeta},\quad \dfrac{\partial}{\partial z} = \dfrac{\partial}{\partial\theta} + q(\rho)\dfrac{\partial}{\partial\zeta}$

safety factor and magnetic shear: $q(\rho) = \dfrac{d\Phi}{d\Psi},\quad \hat{s}(\rho) = \dfrac{\rho}{q}\dfrac{dq}{d\rho}$

Gyrokinetic equation in flux coordinates

- Metric tensor

$$g^{xx} = \nabla x \cdot \nabla x = c_x^2 g^{\rho\rho}$$
$$g^{xy} = \nabla x \cdot \nabla y = c_x c_y [\dot{q}\theta g^{\rho\rho} + q g^{\rho\theta} - g^{\rho\zeta}]$$
$$g^{xz} = \nabla x \cdot \nabla z = c_x g^{\rho\theta}$$
$$g^{yy} = \nabla y \cdot \nabla y = c_y^2 [(\dot{q}\theta)^2 g^{\rho\rho} + q^2 g^{\theta\theta} + g^{\zeta\zeta} + 2q\dot{q}\theta g^{\rho\theta} - 2q g^{\theta\zeta} - 2\dot{q}\theta g^{\rho\zeta}]$$
$$g^{yz} = \nabla y \cdot \nabla z = c_y [\dot{q}\theta g^{\rho\theta} + q g^{\theta\theta} - g^{\theta\zeta}]$$
$$g^{zz} = \nabla z \cdot \nabla z = g^{\theta\theta}$$

- Advection operators in general forms for arbitrary flux coordinate systems:

$$\boldsymbol{b} \cdot \nabla = \frac{c_b}{B\sqrt{g}_{xyz}} \frac{\partial}{\partial z}, \quad k_\perp^2 = k_x^2 g^{xx} + 2k_x k_y g^{xy} + k_y^2 g^{yy}, \quad \frac{1}{L_{n_s}} = -\frac{d \ln n_s}{dx}, \frac{1}{L_{T_s}} = -\frac{d \ln T_s}{dx}$$

$$\boldsymbol{k}_\perp \cdot \boldsymbol{v}_{ds} = \frac{m_s v_\parallel^2 + \mu B}{e_s c_b} [\mathcal{K}_x k_x + \mathcal{K}_y k_y], \quad \boldsymbol{k}_\perp \cdot \boldsymbol{v}_{*s} = -\frac{T_s}{e_s c_b} \left[\frac{1}{L_{n_s}} + \frac{1}{L_{T_s}} \left(\frac{m_s v_\parallel^2}{2T_s} + \frac{\mu B}{T_s} - \frac{3}{2} \right) \right] k_y$$

$$\mathcal{K}_x = \frac{g^{xz} g^{xy} - g^{xx} g^{xz}}{B^2/c_b^2} \frac{\partial \ln B}{\partial z} - \frac{\partial \ln B}{\partial y}, \quad \mathcal{K}_y = \frac{g^{xz} g^{yy} - g^{xy} g^{yz}}{B^2/c_b^2} \frac{\partial \ln B}{\partial z} + \frac{\partial \ln B}{\partial x}$$

---> Only B-intensity, and its derivatives, and the contra-variant metric components are necessary to calculate these operators.

Construction of SFL flux coordinates from MEUDAS

Data flow

MEUDAS (developed in JAEA)

2D Free-boundary Grad-Shafranov solver

$$P = P(\Psi),\ \ I = I(\Psi)$$

$$\Psi = \Psi(R, Z)$$

IGS [Matsuyama]

Flux coordinate Interface

Interpolation, tracing flux surfaces

Constructing Axisymmetric, Hamada, and Boozer coordinates

The radial label :

$$\boxed{\rho = \sqrt{\Phi/\Phi_{\mathrm{edge}}},}\quad \rho = \sqrt{\Psi/\Psi_{\mathrm{edge}}}$$

The minor radius :

$$a = \sqrt{V_{\mathrm{edge}}/2\pi^2 R_{\mathrm{ax}}},\quad \boxed{a = \sqrt{2\Phi_{\mathrm{edge}}/B_{\mathrm{ax}}},}$$

$$a = \sqrt{2\Psi_{\mathrm{edge}}/B_{\mathrm{ax}}}$$

$$R = R[\rho, \theta],\ \ Z = Z[\rho, \theta],\ \ \phi = \zeta - q(\rho)G[\rho, \theta]$$

$$B = B[\rho, \theta],\ \ dB/d\rho,\ \ dB/d\theta$$

GKV

Local fluxtube code

Calculating metric components and advection operators

Turbulence simulation

Co-variant metric components are calculated by

$$g_{ij} = \frac{\partial R}{\partial u_i}\frac{\partial R}{\partial u_j} + \frac{\partial Z}{\partial u_i}\frac{\partial Z}{\partial u_j} + R^2\frac{\partial \phi}{\partial u_i}\frac{\partial \phi}{\partial u_j}$$

$$u_i = \{\rho, \theta, \zeta\}$$

, then converted to contra-variant components.

Verification of flux coordinates with solovev equilibrium

- Analytic expression of solovev equilibrium with finite elongation, triangularity, and up-down asymmetry:

$$\frac{\Psi(\bar{R},\bar{Z})}{\Psi_{\mathrm{edge}}} = \frac{1}{\epsilon_a^2}\left[\frac{(1-d)\bar{R}^2\bar{Z}^2 + d\bar{Z}^2}{E^2} + \frac{1}{4}(\bar{R}^2-1)^2\right] + \frac{\nu_{\mathrm{asym}}}{\epsilon_a}(\bar{R}^2-1)\bar{Z}, \quad \bar{R} = R/R_{\mathrm{ax}}, \bar{Z} = Z/R_{\mathrm{ax}}$$

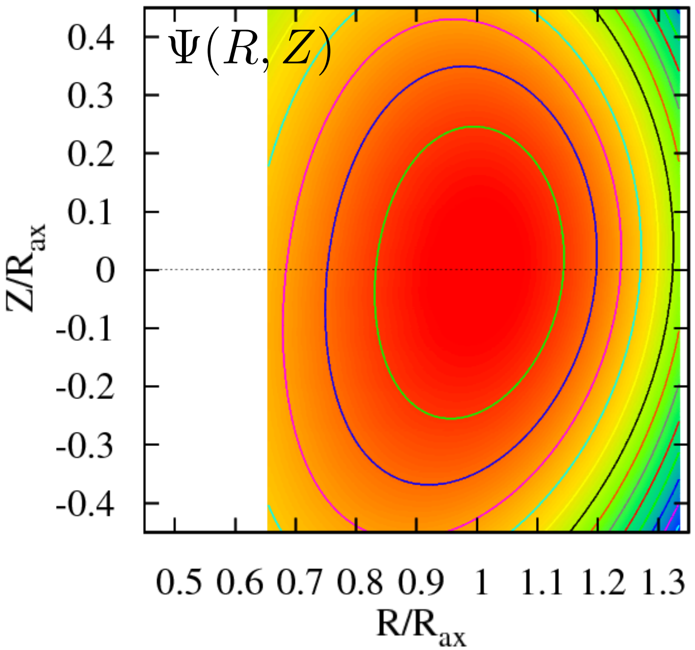

Original 2D equilibrium data with

$E = 1.6,\ d = 0.05,$

$\epsilon_a = 0.25,\ \nu_{\mathrm{asym}} = -0.3$

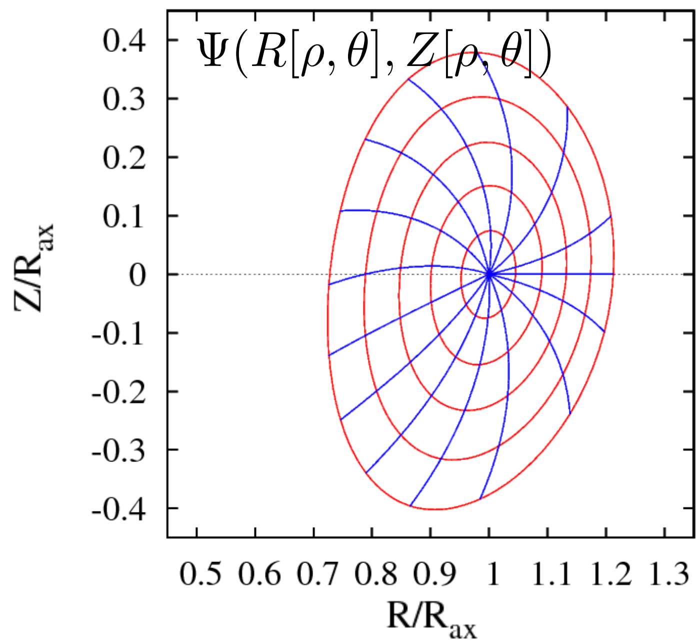

Boozer coord. with $\rho = (\Psi/\Psi_{\mathrm{edge}})^{\frac{1}{2}}$

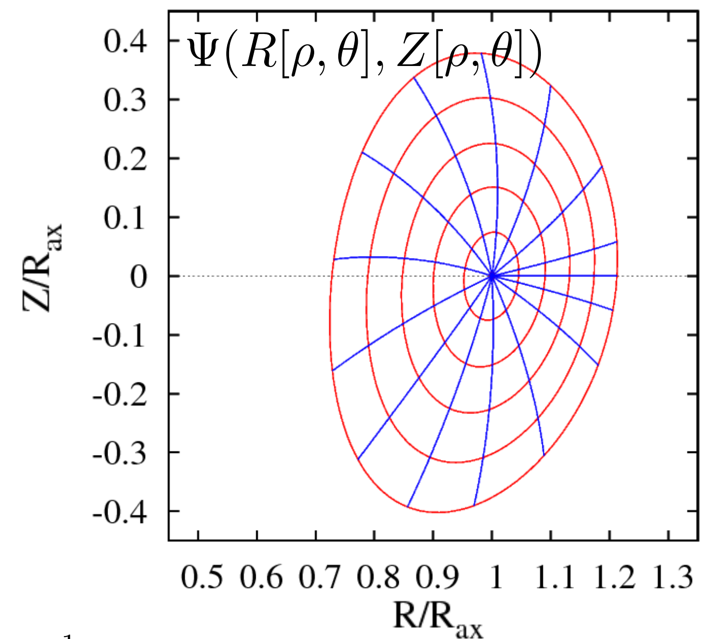

Hamada coord.

Less deformation of constant θ -surface near the edge for Hamada coord. (especially, out-board side)

Verification of flux coordinates with solovev equilibrium

- Consistency is verified by the following analytical expressions:

$$\boxed{\frac{\partial R[\rho,\theta]}{\partial \theta} = -\frac{\sqrt{g}}{R}\frac{\partial \rho(R,Z)}{\partial Z}}$$

$$\boxed{g^{\rho\rho} = \left\| \frac{\partial \rho}{\partial R}\nabla R + \frac{\partial \rho}{\partial Z}\nabla Z \right\|^2}$$

Relative error to analytical expressions

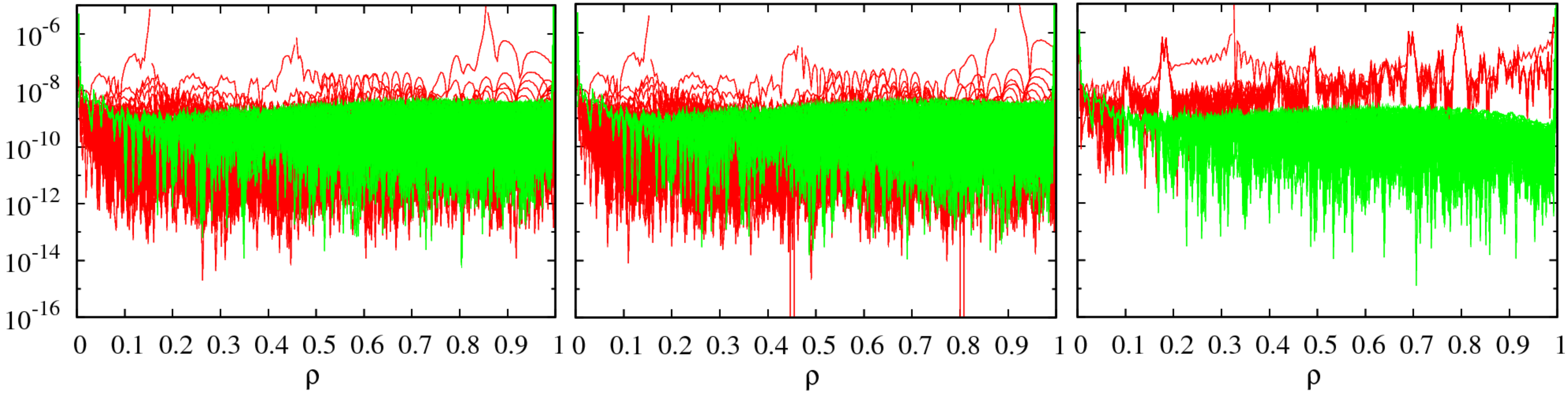

Axisymmetric coord. Boozer coord. Hamada coord.

All the constructed coordinate systems show sufficient accuracy(up to ~10^{-8}) for turbulent transport analyses.

Outline

- Introduction
- Current status of local gyrokinetic Vlasov code GKV
- Interface between MEUDAS(2D equilibrium solver) and GKV
- Application to realistic plasma shapes on JT-60SA
  - Linear ITG mode stability
  - Residual zonal flow levels
  - Nonlinear zonal flow generations
- Summary

Application to realistic plasmas on JT-60SA

- Two L-mode plasmas are considered (The MHD stability has been well investigated: N. Aiba PFR2007):

ITER-like plasma with single null: "IT"

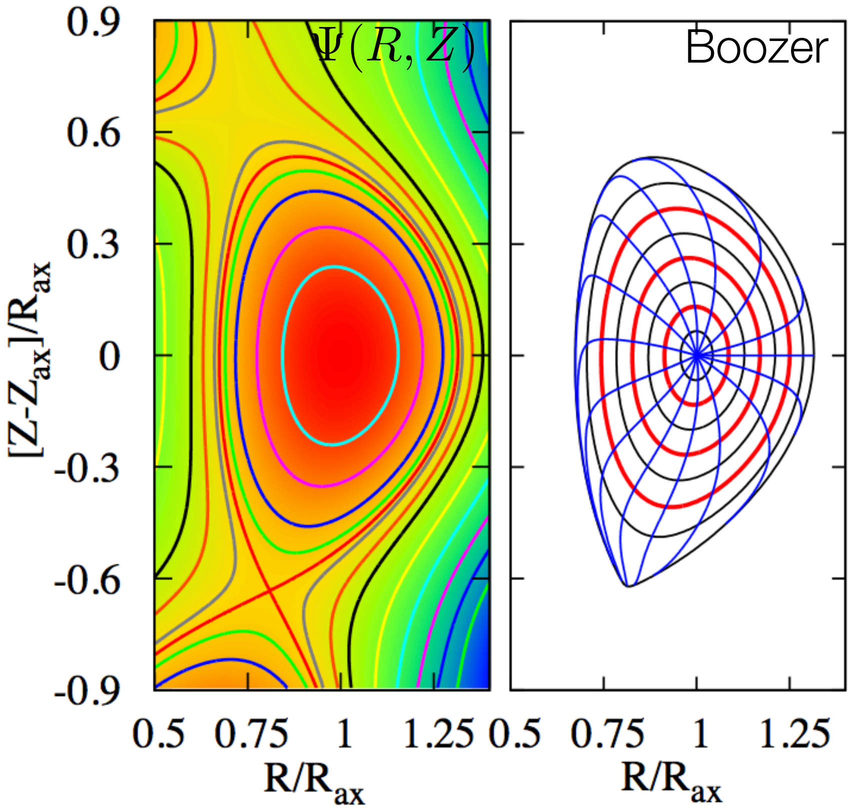

$$R_{\rm ax} = 3.02{\rm m},\ a = 1.29{\rm m},\ V = 90.7{\rm m}^3,$$
$$B_{\rm ax} = 2.64{\rm T},\ q_{\rm ax} = 1.82,\ q_{95} = 3.88,$$
$$I_{\rm p} = 2.59{\rm MA},\ S = q_{95} I_{\rm p}/B_{\rm ax} a = 2.95$$

Highly-Shaped plasma with quasi double null: "HS"

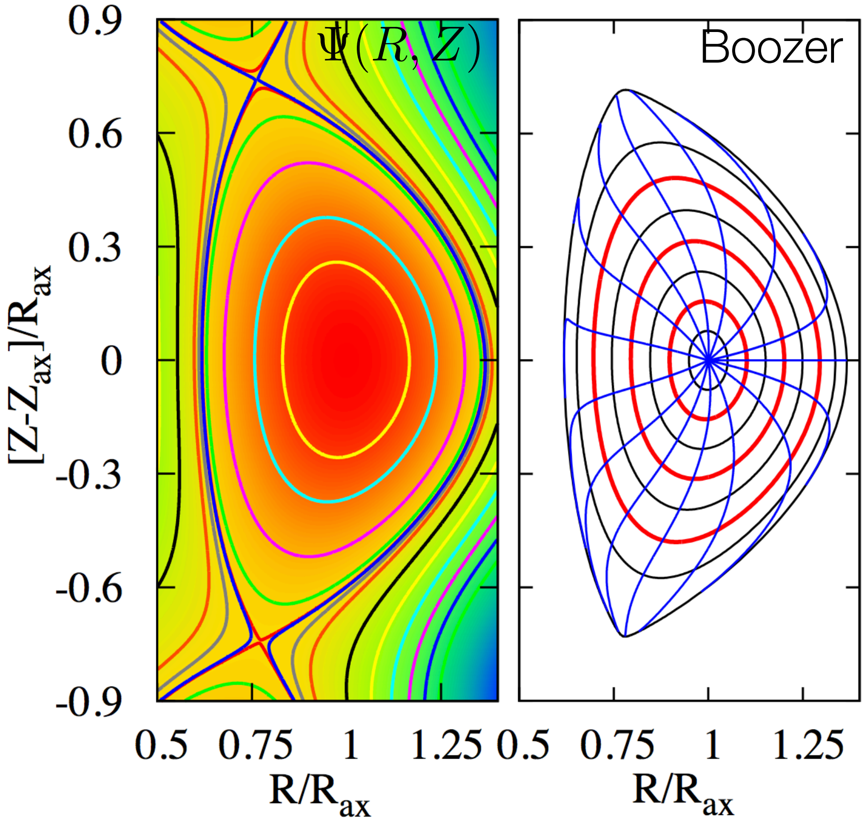

$$R_{\rm ax} = 3.05{\rm m},\ a = 1.53{\rm m},\ V = 129.5{\rm m}^3,$$
$$B_{\rm ax} = 2.88{\rm T},\ q_{\rm ax} = 1.41,\ q_{95} = 3.59,$$
$$I_{\rm p} = 5.00{\rm MA},\ S = q_{95} I_{\rm p}/B_{\rm ax} a = 4.07$$

Field aligned structures of B-intensity, ω_d, and k^2

IT: ITER-like, HS: Highly shaped

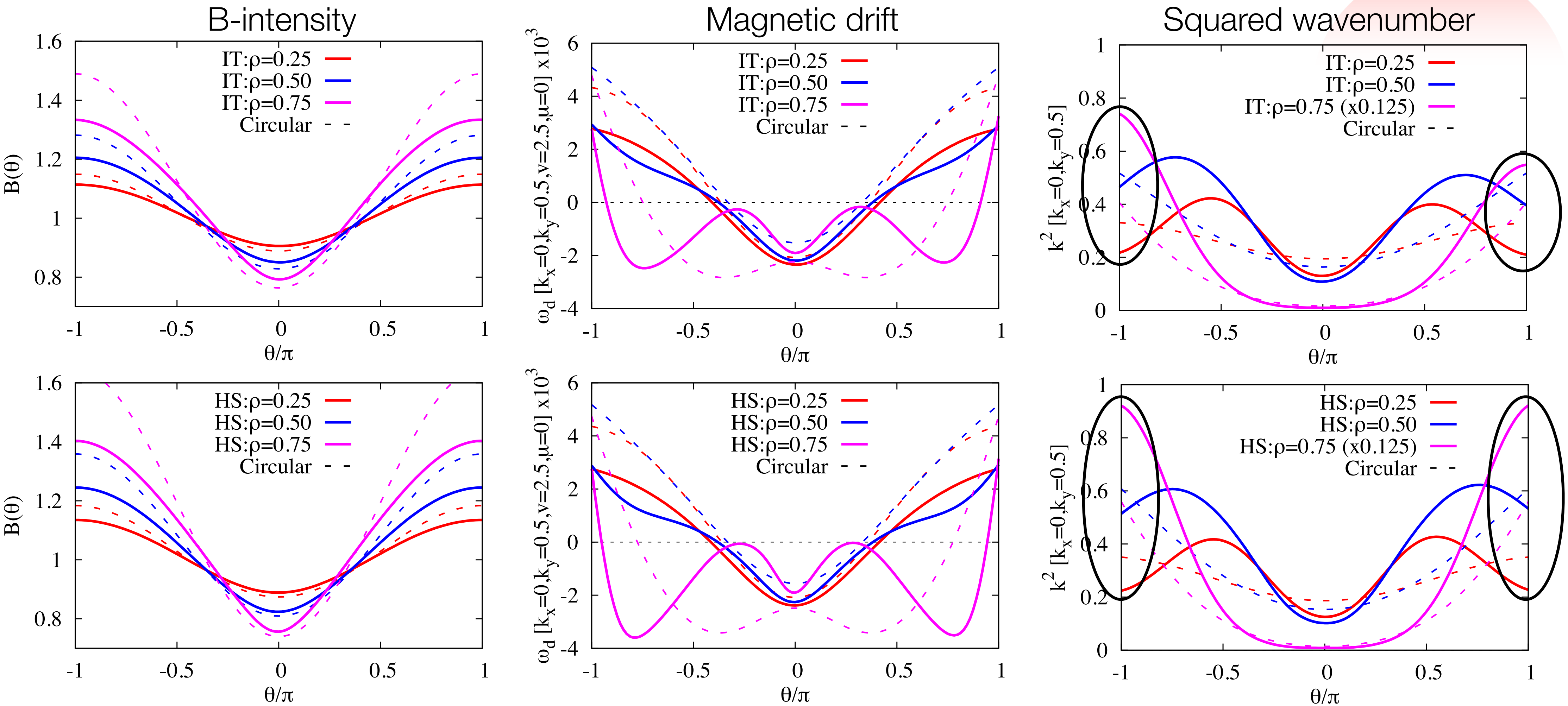

- Field aligned structures in shaped plasmas deviate from those in circular plasmas (outer sides).
- Stronger asymmetry in k^2 for ITER-like plasma than that in Highly-Shaped plasma.

Trapped/Passing boundaries

IT: ITER-like, HS: Highly shaped

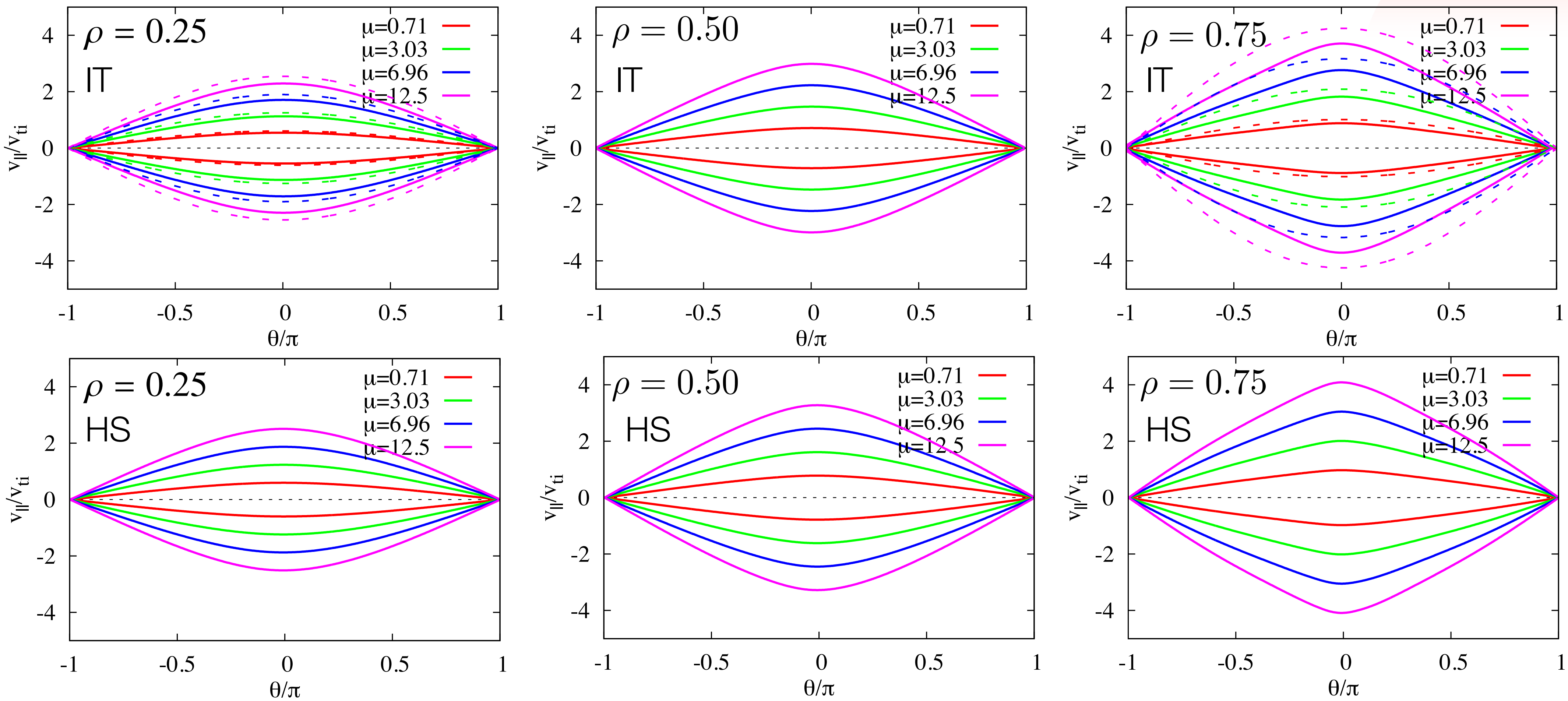

- More sharp boundary, but less trapped region for shaped plasmas compared with circular ones.

---> Strong impacts on ITG with kinetic elec. and TEM turbulence dynamics.

Linear ITG mode stability for the ITER-like plasma

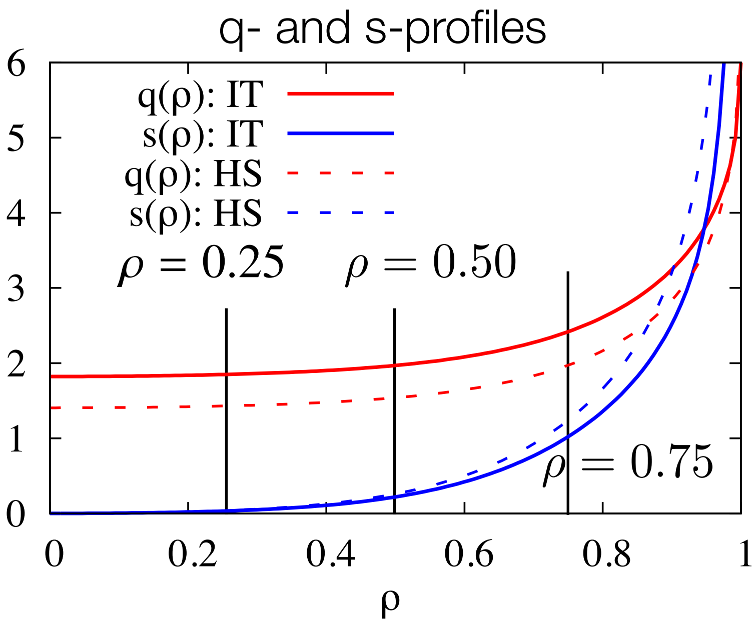

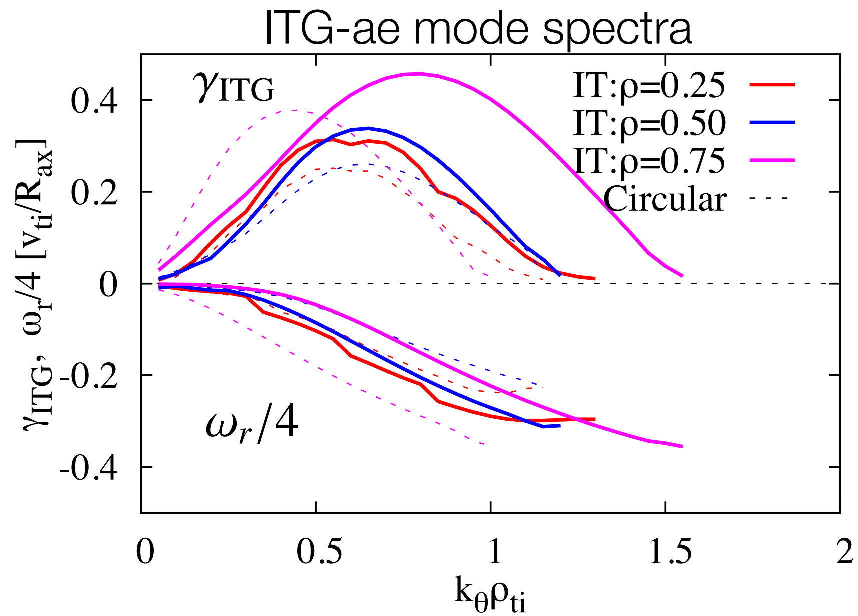

IT	0.25	0.50	0.75
r/R_{ax}	0.104	0.214	0.322
q	1.85	1.97	2.43
s	0.03	0.23	1.06

$R_{\rm ax}/L_n = 3.0,\ R_{\rm ax}/L_T = 6.0,$
$T_{\rm e}/T_{\rm i} = 1, k_{y(\rm min)} = 0.05$

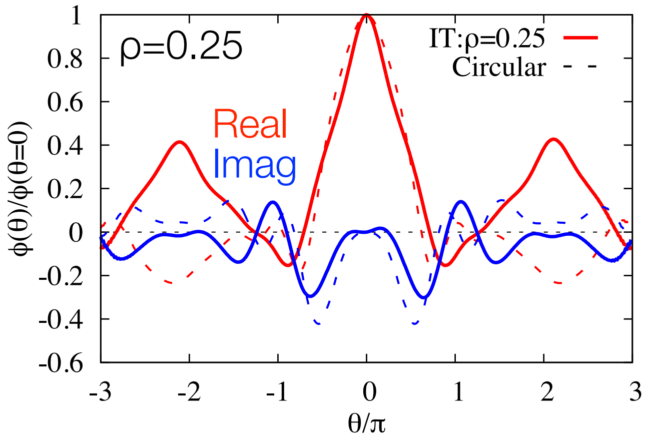

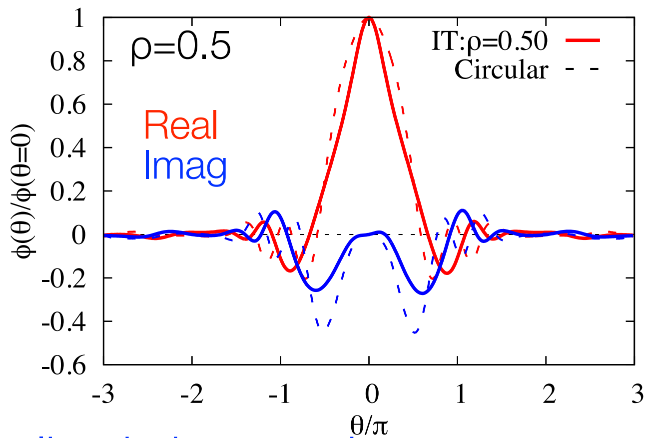

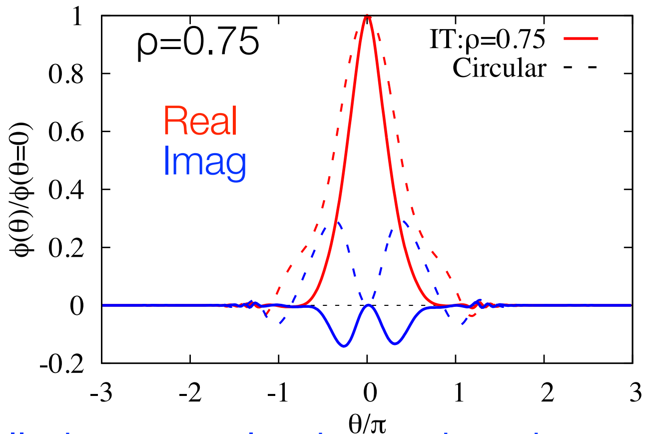

- Broader ITG-spectra with more localized eigenmode appear especially in strongly shaped region (outer side).

Linear ITG mode stability for the Highly-Shaped plasma

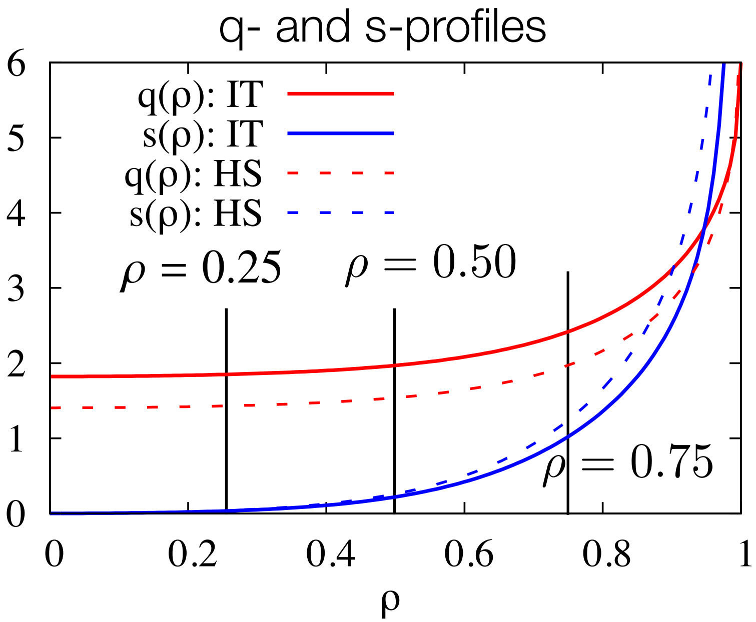

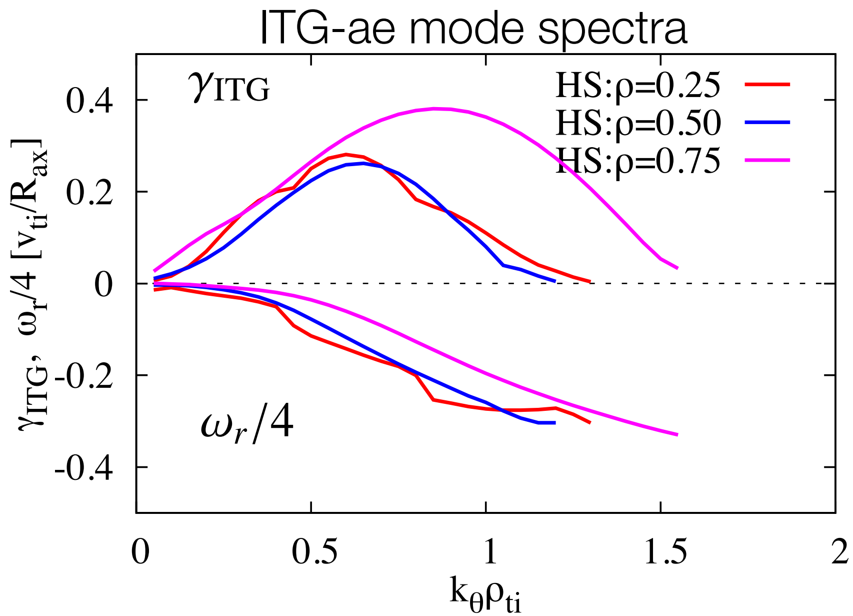

HS	0.25	0.50	0.75
r/R_{ax}	0.123	0.250	0.38
q	1.43	1.54	1.97
s	0.03	0.35	1.23

$R_{ax}/L_n = 3.0,\ R_{ax}/L_T = 6.0,$
$T_e/T_i = 1, k_{y(\min)} = 0.05$

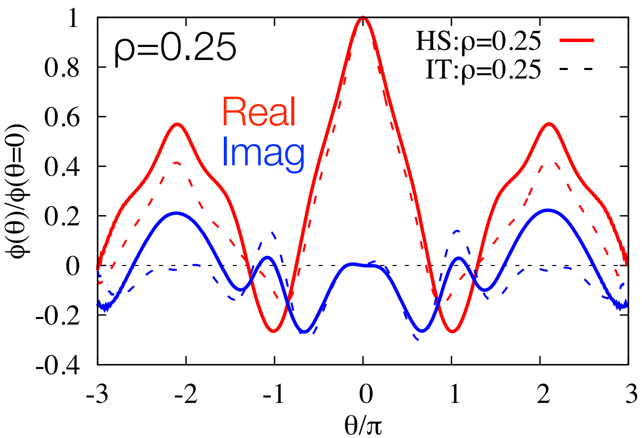

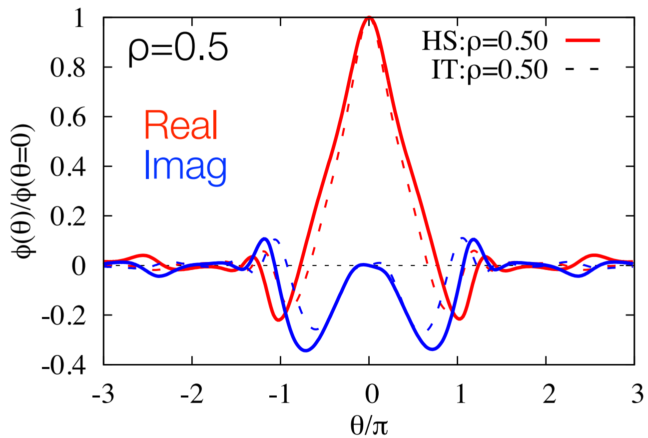

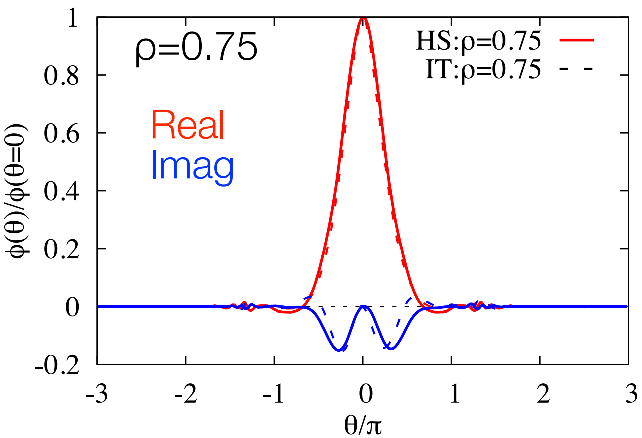

- ITG mode growth rates in Highly-shaped case is slightly lower than those in the ITER-like cases.

Geometric dependence of residual zonal flow levels

IT: ITER-like, HS: Highly shaped

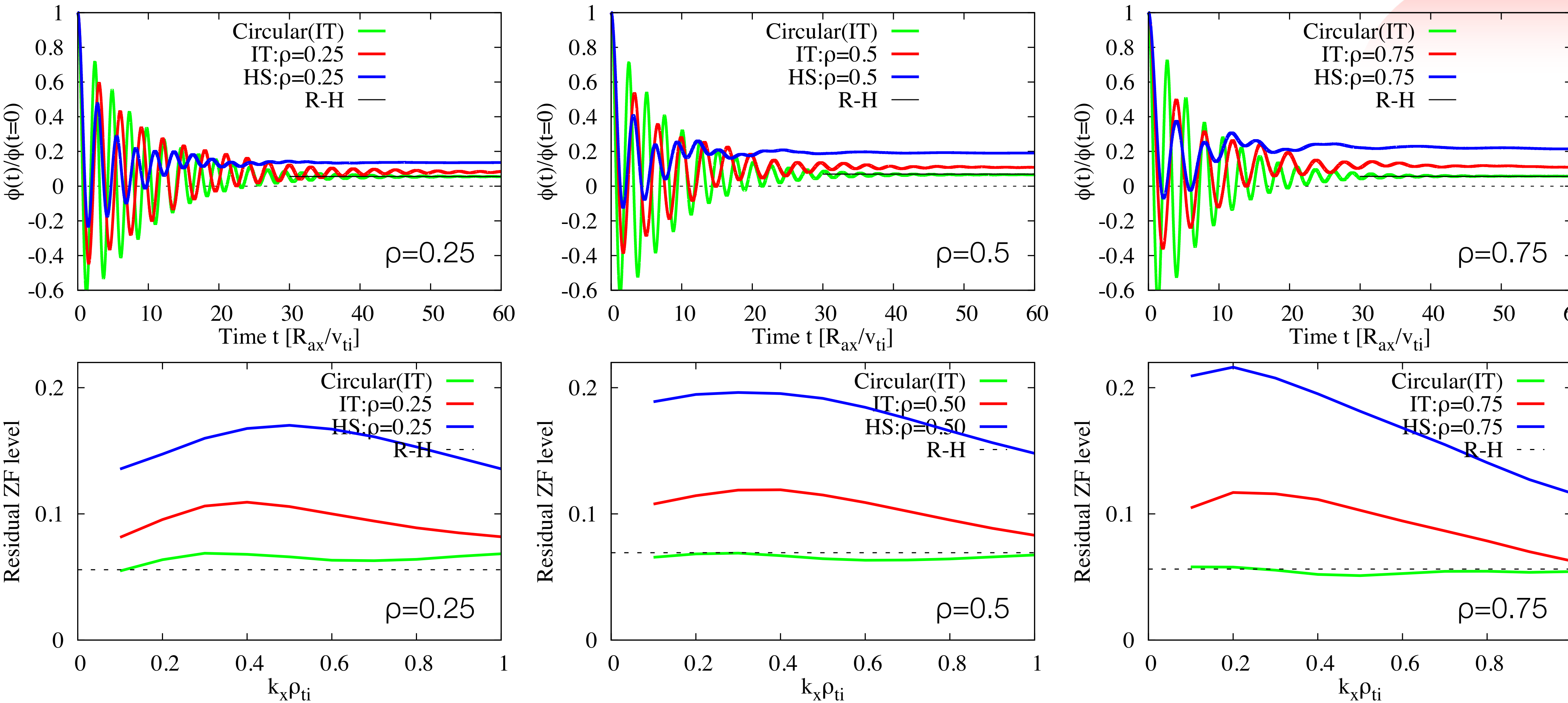

- Shaping effects in IT- and HS- plasmas lead to
  ---> significant enhancement of residual zonal flow levels
  ---> stronger k_x- (or k_r-) dependence compared with circular plasmas.

HS is expected to be more favorable to ITG-stability and ZF-response!

Outline

- Introduction
- Current status of local gyrokinetic Vlasov code GKV
- Interface between MEUDAS(2D equilibrium solver) and GKV
- Application to realistic plasma shapes on JT-60SA
  - Linear ITG mode stability
  - Residual zonal flow levels
  - Nonlinear zonal flow generations
- Summary

Nonlinear simulation and entropy balance

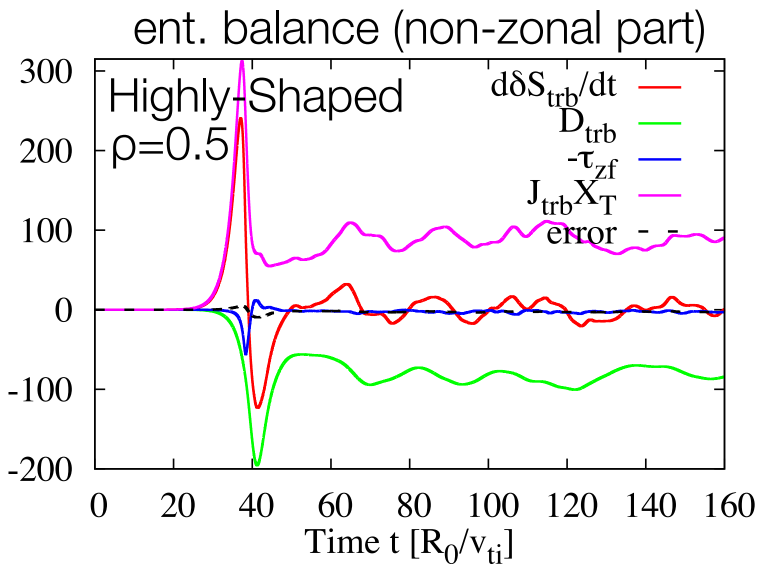

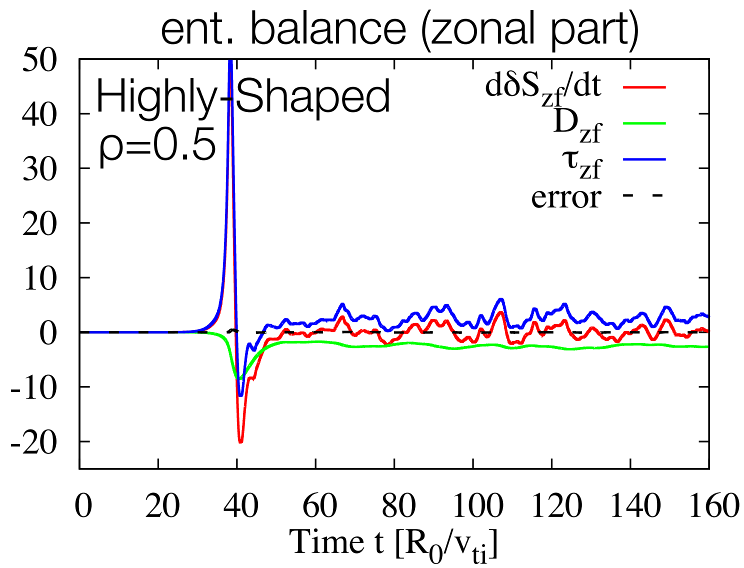

entropy variable

col. dissipation

$$\frac{d\delta S_{trb}}{dt} = J_{trb}X_T - \tau_{zf} + D_{trb}$$

(flux) x (thermo. force)

$$\frac{d\delta S_{zf}}{dt} = \tau_{zf} + D_{zf}$$

transfer from NZ to Z

- The entropy balance relations are well satisfied both in the non-zonal and zonal parts.

- Highly-Shaped cases show lower transport levels with higher critical temperature gradient.

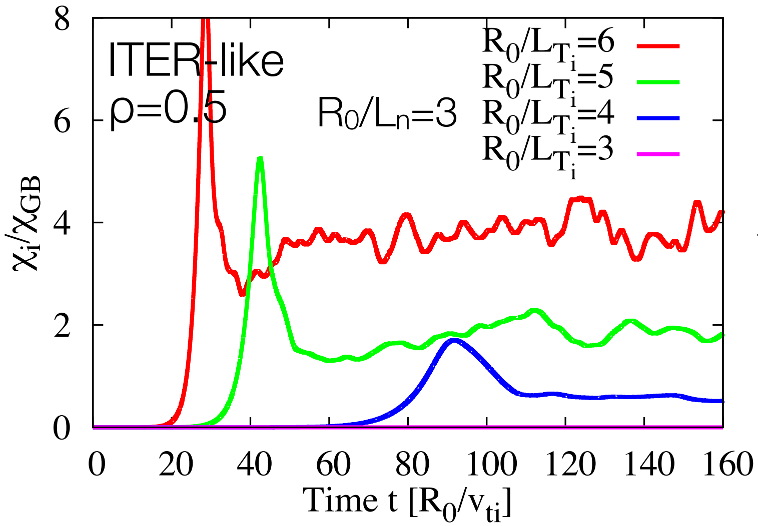

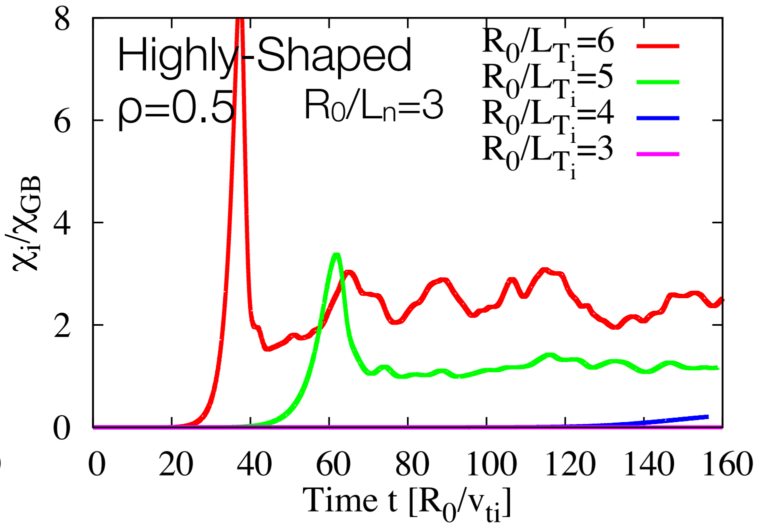

Nonlinear zonal flow generation

IT: ITER-like, HS: Highly shaped

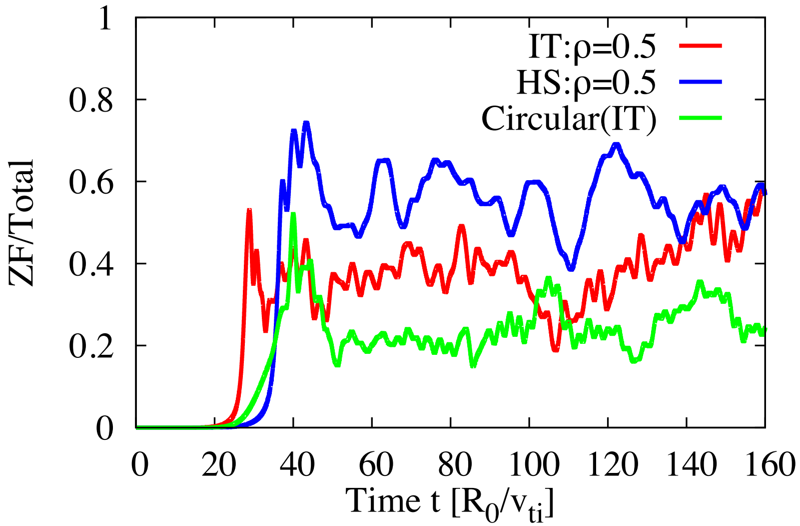

Snapshots of the potential fluctuation

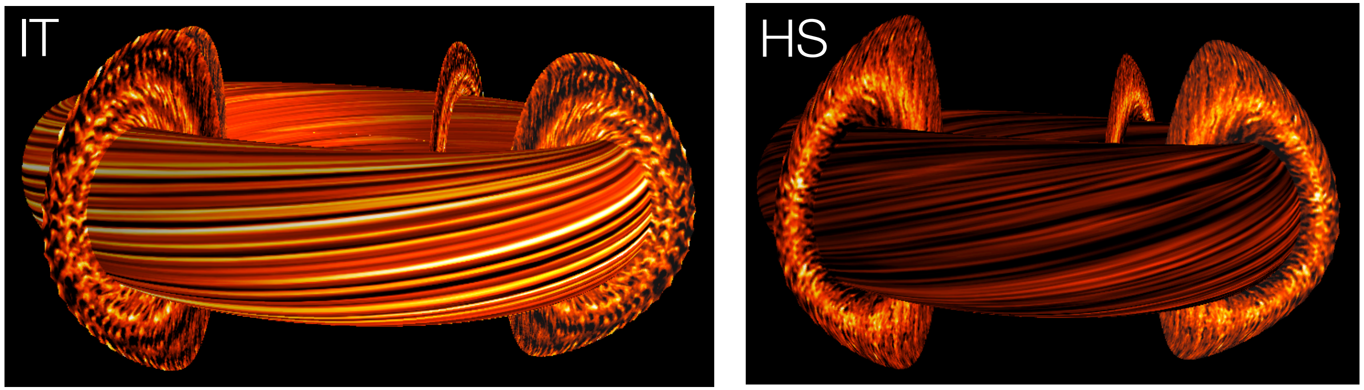

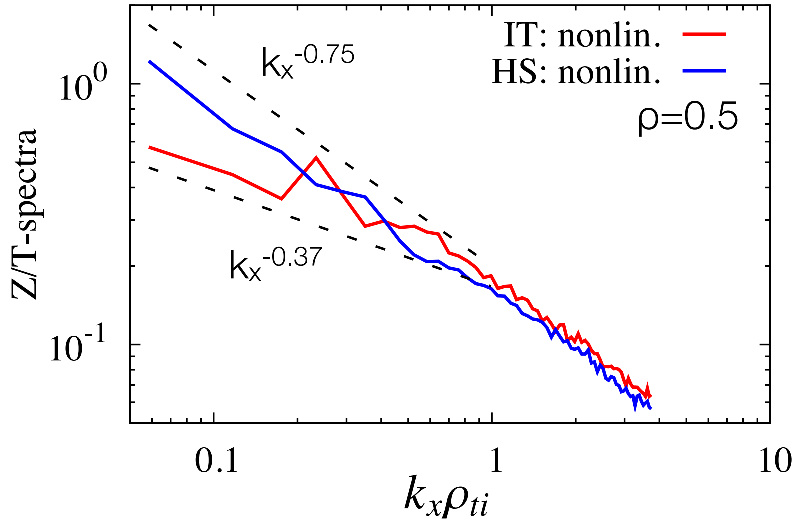

- As is expected by linear ZF-damping analyses, more efficient ZF generation is observed in the nonlinear phase of the Highly-Shaped case.

- Stronger k_x-dependence of Z/T is also identified in the Highly-Shaped case. (Z: ZF-intensity, T: turbulence intensity)

---> Qualitative features on the amplitude and k_x-dependence are well agreed with linear results shown in the previous slides.

Towards the transport modeling

- ITG turbulence simulations on LHD show that the ion heat diffusivity well scales with $T/Z^{1/2}$, and GK-simulation-based transport model including zonal-flow effects has been developed.

[M. Nunami PoP2012, 2013]

Scaling on LHD [M. Nunami PoP2012] and JT-60SA

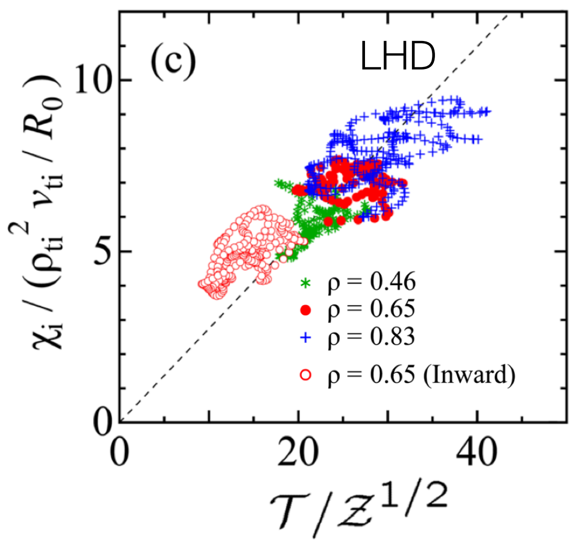

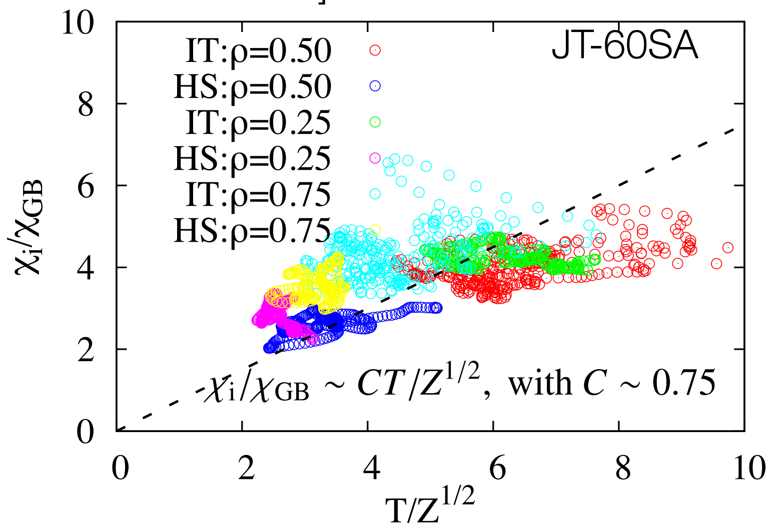

Turbulence spectra

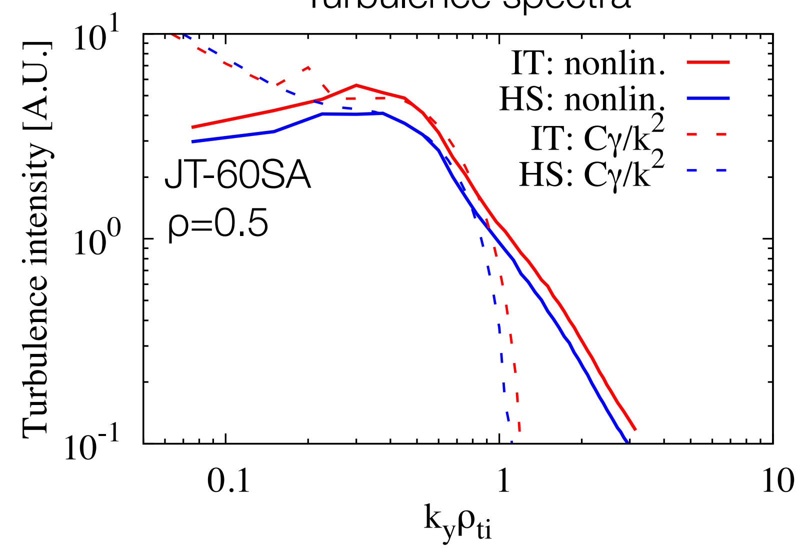

- Good scaling between χi and $T/Z^{1/2}$ is also observed in JT-60SA case.

- Turbulence spectra near the peak region are well characterized with linear spectra, $\gamma_{\mathrm{ITG}}/k_y^2$.

---> Promising to construct the similar reduced transport model produced by the linear spectra and residual ZF levels. (currently underway...)

Summary

- An interface code to generate flux coordinates system from realistic plasma equilibria calculated by free-boundary 2D Grad-Shafranov solver MEUDAS is successfully implemented to a local fluxtube code GKV.

- The accuracy of the flux coordinates, i.e., Axisymmetric, Boozer, and Hamada, are verified with an analytical solovev equilibrium model.

- Linear ITG-ae stability (ae: adiabatic electrons) is investigated for two types of shaped plasmas in JT-60SA, i.e., ITER-like plasma(IT) and Highly shaped one(HS), then the difference from the concentric circular equilibrium, which is conventionally used in gyrokinetic code, has been clarified.

---> Highly-shaped configuration shows less ITG-driven transport than that in the standard ITER-like configuration, due to stronger generation of zonal flows.

---> The turbulent ion heat diffusivity well scales with $T/Z^{1/2}$, which suggests the applicability of a GK-simulation based transport model.

More detailed analyses including a multi-species/scales stability analysis, nonlinear simulations, and constructing the GK-based transport model are in progress.